J. Braz. Chem. Soc., Vol. 17, No. 7, 1419-1427, 2006.
Printed in Brazil - ©2006 Sociedade Brasileira de Química
0103 - 5053 $6.00+0.00

Article

Structural and Morphological Investigations of the Electrodeposited Cr and Ni-Cr-P Coatings and their Electrochemical Behaviors in Chloride Aqueous Medium

Pedro de Lima-Neto,* Adriana N. Correia and Gecílio P. da Silva

Departamento de Química Analítica e Físico-Química, Universidade Federal do Ceará, Campus do Pici, Bloco 940, 60455-970 Fortaleza-CE, Brazil

Neste trabalho foi estudada a influência dos parâmetros operacionais de eletrodeposição na estrutura, na morfologia dos revestimentos de Cr e Ni-Cr-P e no comportamento eletroquímico destes em meio aquoso contendo cloreto. Todos os eletrodepósitos foram obtidos sobre cobre. As camadas de Cr foram obtidas a partir de um banho industrial. Os eletrodepósitos amorfos de Ni-Cr-P foram obtidos a 60 °C, no intervalo de 100 a 400 mA cm^{-2} e usando um banho de pH igual a 2 e contendo: 40 g L^{-1} de $NiCl_2.6H_2O$; 102 g L^{-1} de $CrCl_3$; 14 g L^{-1} de $NaPH_2O_2$; 30 g L^{-1} de H_3BO_3; 15 g L^{-1} de NaBr; 50 g L^{-1} de NH_4Cl, 80 g L^{-1} de $Na_3C_6H_5O_7.2H_2O$ e 40 mL L^{-1} de HCOOH. Estas camadas foram obtidas com cargas de eletrodeposição de 500 e 1600 Coulombs A caracterização dos eletrodepósitos foi feita por Calorimetria de Varredura Diferencial (DSC), Difração de Raios X (XRD), Microscopia Eletrônica de Varredura (SEM) e Energia Dispersiva de Raios X (EDX). O comportamento eletroquímico foi avaliado por polarização potenciodinâmica em NaCl 0,1 mol L^{-1} e à temperatura ambiente. Não foi observada a presença de trincas nas camadas eletrodepositadas de Ni-Cr-P e a morfologia superficial foi caracterizada pela presença de nódulos esféricos. A cristalização das ligas de Ni-Cr-P ocorreu a 325 °C com a formação de fases de Ni e Ni_3P. O eletrodepósito de cromo não apresentou trincas, mas todos os revestimentos de Cr que foram tratados termicamente apresentaram trincas distribuídas por toda a superfície e apresentaram diminuição na dureza e na resistência à corrosão. A dureza das camadas de Ni-Cr-P aumentou com a temperatura de tratamento térmico e este comportamento foi associado à presença da fase Ni_3P. A morfologia nodular desapareceu durante o tratamento térmico e foi relacionada à difusão de Cr para a superfície. Dentre os vários eletrodepósitos de Ni-Cr-P estudados, a camada $Ni_{66}Cr_{12}P_{22}$ foi a que apresentou melhor resistência à corrosão e com um potencial de corrosão ligeiramente superior ao apresentado pelo eletrodepósito de Cr. O revestimento $Ni_{66}Cr_{12}P_{22}$ é um potencial candidato a substituir o revestimento de Cr industrial, principalmente sob condições operacionais em temperaturas superiores à ambiente.

Structural and morphological characteristics of the electrodeposited Cr and Ni-Cr-P coatings and their corresponding electrochemical behaviors in chloride aqueous medium were investigated here. All coatings were electrodeposited on copper. Cr coatings were obtained from an industrial plating solution and amorphous Ni-Cr-P coatings were successfully obtained at 60ºC in the range of 100 to 400 mA cm^{-2}, using a plating solution at pH 2 containing 40 g L^{-1} $NiCl_2.6H_2O$; 102 g L^{-1} $CrCl_3$; 14 g L^{-1} $NaPH_2O_2$; 30 g L^{-1} H_3BO_3; 15 g L^{-1} NaBr; 50 g L^{-1} NH_4Cl, 80 g L^{-1} $Na_3C_6H_5O_7.2H_2O$ and 40 mL L^{-1} HCOOH. The coatings were obtained using constant charges of 500 and 1600 Coulombs. The characterization of the coatings was carried out by Scanning Electron Microscopy (SEM), X-ray Diffraction (XRD), Differential Scanning Calorimetry (DSC) and Energy Dispersive X-ray Analysis (EDX) techniques. The electrochemical behavior of both coatings was evaluated by potentiodynamic polarization curves, at room temperature, in 0.1 mol L^{-1} NaCl aqueous solution. It was not observed cracks on the electrodeposited Ni-Cr-P coatings and the surface morphology was characterized by the presence of spherical nodules. The crystallization of these coatings occurred at 325 °C with the formation of Ni and Ni_3P phases. All the annealed Cr coatings showed cracked surfaces. The presence of cracks impairs the mechanical and corrosion resistance properties of Cr coatings. The hardness of the Ni-Cr-P was increased with the increase of the annealing temperature**.** Spherical noodles were absent in the surface of as-annealed Ni-Cr-P coating which it was associated with the diffusion of Cr to the surface and cracks were not observed in any annealing temperature. Among the various electrodeposited Ni-Cr-P coatings studied here, the $Ni_{66}Cr_{12}P_{22}$ coating presented the best corrosion behavior and it is a potential candidate to substitute Cr in industrial application, mainly at operational temperatures that exceed room temperature.

Keywords: corrosion, crystallization behavior, hardness, Ni-Cr-P, Cr

*e-mail: pln@ufc.br

Introduction

Electrodeposited chromium coating is widely used as both decorative and functional coating because it presents good properties such as high hardness, good wear resistance, low coefficient of friction and excellent corrosion resistance, when used for industrial applications at room temperature. However, its industrial application has been limited by public health and environmental laws because conventional industrial Cr galvanization process requires the use of carcinogenic Cr^{6+} ions in the chromium plating bath, and also because the hardness and corrosion resistance of this coating decrease when the operating temperature exceeds the room temperature.[1]

Thereby, the investigation about environmental acceptable alternative coatings to electrodeposited chromium coatings has increased and a review about this subject is given by Brooman.[2,3] Among the possible alternatives, electrodeposited Ni-Cr coatings obtained from a trivalent chromium plating bath are interesting and safe because Cr^{3+} ions are non-toxic. Additionally, these electrodeposited coatings have exhibited good corrosion resistance and retaining the strength and hardness at high temperature.[4]

On the other hand, amorphous metallic alloys present interesting mechanical, magnetic and electrochemical properties. The physicochemical processing and technical application of the amorphous metallic alloys have been reviewed by some authors.[5-8] These materials have shown higher corrosion resistance than the crystalline alloys with the same composition, encouraging the interest to produce anticorrosive amorphous coatings. This class of coating can be produced by sputtering, electroless and electrodeposition techniques.[9-16] Among these techniques, electrodeposition technique is very suitable to produce amorphous coatings because it permits to work with substrates in different shapes and geometries and makes it possible to control the thickness and the composition of the coating only changing the electrodeposition parameters.

Ni-P was the first amorphous alloys used in industrial application as protective coating in many corrosive environments such as food industry, oil and gas industries, aerospace and automotive industries.[9] Additionally, the co-electrodeposition of a third element to form a ternary electrodeposited Ni-P-based amorphous coating has produced new coatings with higher corrosion resistance than the electrodeposited Ni-P amorphous coating, as shown in a previous work.[10]

Amorphous metallic alloys containing Cr co-electrodeposited with metals belonging to the iron group of the periodic table were successfully reported in the literature.[11-16] Consequently, the increasing interest in the Ni-Cr-P amorphous coating has been evidenced and it is possible to find reports in the literature discussing the evolution of the structure and the microhardness during annealing of sputtered Ni-Cr-P.[15,16] Although this coating appears as a possible candidate to replace the industrial hard chromium coating, little data in the literature are reported about the influence of the operational parameters in the electrodeposition of this coating and the influence of the annealing temperature on the structure and surface morphology of the electrodeposited Ni-Cr-P coating has not been investigated yet, and its corrosion behavior in aqueous medium is little known.

Thus, this work purported to compare the structural, morphological and electrochemical properties of the electrodeposited Cr and Ni-Cr-P coatings. An analysis of the influence of thermal treatments on the structure, surface morphology, and microhardness of these coatings was also included.

Experimental

Electrodeposition

For the preparation of the electrodeposition bath and corrosion testing solutions the water was purified by Milli-Q plus system and analytical grade chemicals reagents were used. All coatings were electrodeposited on a copper disc, embedded in epoxy resin exposing a geometric area of approximately 1 cm^2. Electrodepositions were carried out in a one-compartment cell made of Pyrex® glass and with Teflon® cover having adequate holes to lodge the electrodes keeping a parallel plane between the Cu cathode and the Pt foil anode with 2 cm^2 of geometric area. Prior to the plating, the copper surface was polished with 240, 400 and 600 SiC emery paper, degreased in hot NaOH solution, rinsed in distilled water, etched in 15% HCl solution and, finally, rinsed with distilled water.

The composition of the plating solution and the operational parameters used to deposit Ni-Cr-P coatings are shown in Table 1. The Cr coatings were deposited under galvanostatic control at 135 mA cm^{-2} from an industrial plating bath containing 180 g L^{-1} CrO_3 and 1 g L^{-1} H_2SO_4, at 60 °C.[17]

Characterization

Surface and cross section morphologies and the coatings thickness of the samples were analyzed by scanning electron microscopy (SEM) using a Philips XL-

Table 1. Plating solution composition and operational parameters for Ni-Cr-P deposition

Reagent	Concentration
$NiCl_2.6H_2O$ (Nickel Chloride)	40 g L^{-1}
$CrCl_3.6H_2O$ (Chromium Chloride)	102 g L^{-1}
H_3BO_3 (Boric Acid)	30 g L^{-1}
NaH_2PO_2 (Sodium Hypophosphite)	14 g L^{-1}
NaBr (Sodium Chloride)	15 g L^{-1}
NH_4Cl (Amonium Chloride)	50 g L^{-1}
$Na_3C_6H_5O_7.2H_2O$ (Sodium Citrate)	80 g L^{-1}
HCOOH (Formic Acid)	40 mL L^{-1}

Operational deposition parameter: pH = 2.0; T = 60 °C; i_d = 100; 200, 300 and 400 mA cm^{-2}. Total charge = 500 and 1600 C.

30 microscope. The SEM cross-section analysis also made possible to measure the average thickness of coatings taken measurements at different points of the coating. Chemical composition of the electrodeposits was determined using a Link Analytical QX-2000 X-ray dispersive analyzer attached to the SEM apparatus. The structure of the as-electrodeposited and as-annealed Ni-Cr-P and Cr coatings was assessed by X-ray diffraction technique (XRD) using a Phillips X' Pert-Pro using a Cu K_a at 40 KV and 40 mA with an incident angle of 3 degrees.

Ni-Cr-P and Cr coatings substrate free, obtained by the copper dissolution immersing the as-electrodeposited samples in a 38% (m/v) $FeCl_3$ aqueous solution, were analyzed by differential scanning calorimetry (DSC). DSC curves were obtained at a heating rate of 10 °C min^{-1} with a N_2 flux of 50 mL min^{-1}, using a SHIMADZU DSC-50 system. As-electrodeposited Cu/Ni-Cr-P and Cu/Cr samples were annealed in a N_2 atmosphere at temperatures selected from the DSC curves, using a heating rate of 10 °C min^{-1} from room temperature to the desired temperature plateau, where they were held for 1 h and then cooled to room temperature. The microhardness of the as-electrodeposited and as-annealed samples was measured with a Shimadzu model HMV-2 Micro Hardness Tester operating with an applied load of 10 g (98.07 mN), which was maintained for 30 s. In order to prevent the effect of the substrate on the microhardness measurements, samples were obtained with a total electrodeposition charge of 1600 C, producing coatings with a thickness of at least 20 μm.

Electrochemical measurements

All electrochemical corrosion tests were conducted in an aerated 0.1 mol L^{-1} NaCl aqueous solution, at room temperature (≅ 27 °C) and in a conventional three-electrode cell, with at least triplicate samples. Pt foil and saturated calomel (SCE) were the auxiliary and reference electrodes, respectively. Potentiodynamic polarization experiments were carried out and using a scan rate of 1 mV s^{-1}. For the electrochemical data acquisition a potentiostat/galvanostat AUTOLAB PGSTAT 30, linked with a PC microcomputer and controlled by the GPES software was used.

Results and Discussion

Influence of the plating parameters

Oxygen was qualitatively detected by the EDX analyses of all the electrodeposited coatings studied here. Some authors[18,19] investigated the electrodeposition of Cr and observed the formation of an amorphous chromic chromate film, $Cr(OH)_3Cr(OH)CrO_4$, following the hydrogen evolution reaction. By means of XPS measurements, Feliciano *et al.*[20] identified the presence of CrO-OH species in the electrodeposited Cr coating. Thus, the identification of this chemical element in the EDX spectra is an indicative of the formation of oxides during the electrodeposition process, as a consequence of the increase of the pH at the metal-solution interface due to the hydrogen evolution.

The influence of the deposition current density on the coating composition, cathodic efficiency and thickness are shown in Table 2. The chemical composition of the Ni-Cr-P was determined from EDX spectra analyses without considering the amount of oxygen, while the cathodic efficiency for Ni-Cr-P electrodeposition was determined from the ratio between the coating thickness measured from the cross section SEM images and the coating thickness given by the Faraday equation. The thickness and cathodic efficiency for the Cr electrodeposition were 7 μm and 10.5%, respectively. This cathodic efficiency is in close agreement with that reported in the literature,[17] which is about 12% for the conventional Cr baths.

The results from Table 2 show that Ni and P contents in the coating increase, while Cr content decreases with current density. Dolati *et al.*[21] studied the electrodeposition of quaternary Fe-Cr-Ni-Mo alloys and observed that the Cr content in the electrodeposited coating decreases as the pH bath increases. In our case, the effect of rising the

Table 2. Influence of the applied deposition current density on composition, on thickness and on cathodic efficiency of Ni-Cr-P alloys

I / (mA cm^{-2})	Composition / at%	Thickness / mm	Efficiency /%
100	$Ni_{66}Cr_{12}P_{22}$	7	4
200	$Ni_{68}Cr_7P_{25}$	3	2
300	$Ni_{68}Cr_6P_{26}$	3	1
400	$Ni_{71}Cr_2P_{27}$	2	1

current density leads to an increase in hydrogen evolution, thus increasing the pH at the interface, which can explain the observed decrease of the Cr content upon increasing the deposition current density, as shown in Table 2.

Table 2 also shows that the thickness declined with the current density, while the cathodic efficiency is low and decreased in the range of 100-300 mA cm^{-2}, remaining constant for higher current densities. Possible explanations for the low cathodic efficiency are: the rising in the hydrogen evolution with the increase of the current density, the formation of metal oxides due to the rising of the pH metal-solution interface during the Ni-Cr-P and Cr electrodeposition process, and the presence of organic ligands, such as citrate and formate, which act as complexing agents of both nickel and chromium ions, forming stable metal complexes that hinder the alloys deposition. The low values of the cathodic efficiency are congruent with some reports published in the literature about the electrodeposition of amorphous metallic alloys contain Cr.[12,13] Lalvani and co-workers[12,13] carried out a systematic investigation of Fe-Cr-P-C and Fe-Ni-Cr-based alloys using Nafion® selective membrane separating the cathode from the anode and they found a maximum cathodic efficiency of 10% in the case of Fe-Cr-P-C alloys and values of cathodic efficiency in the range of 7% to 41% for Fe-Ni-Cr-based alloys. Additionally, Tsai and Wu investigated the electrodeposition of Cr-Ni-C alloys[11] and they found a maximum cathodic efficiency of 11.7%.

Structural investigation

X-ray diffractograms of the electrodeposited Ni-Cr-P coatings are presented in Figure 1. All diffractograms present a broad peak around 2θ of 45°, indicating that Ni-Cr-P amorphous coatings were successfully obtained in all the experimental conditions used. The thermal stability of the Ni-Cr-P coating without the substrate was evaluated by DSC technique and a typical DSC curve is shown in Figure 2. This plot shows two well defined exothermic peaks at 159 °C and at 325 °C and a poorly defined third peak at 477 °C. In the case of Cr film (Figure 2b), the DSC plot presented only an endothermic peak at 118 °C. The formation of unstable chromium hydrides during the chromium plating operation is reported in the literature.[23] These hydrides can be electrodeposited in either hexagonal crystal form or the fcc crystal form. Thus, the peak observed at 118 °C is probably associated with desorption of hydrogen which is added to the coating during the plating process.

In order to evaluate the structural modification with the annealing temperature, Cu/$Ni_{66}Cr_{12}P_{22}$-coated and Cu/

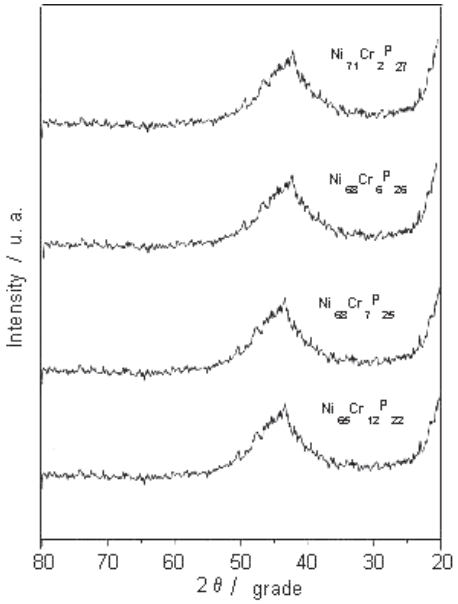

Figure 1. XRD diffraction patterns of the as-electrodeposited Ni-Cr-P coatings.

Cr-coated samples were heat treated at temperatures selected from DSC plots. The evolution of the X-rays diffractograms with the annealing temperature for Cu/$Ni_{66}Cr_{12}P_{22}$-coated sample is shown in Figure 3. As observed, the Cu/$Ni_{66}Cr_{12}P_{22}$-coated sample heat treated at 200 °C and the as-electrodeposited one presented similar X-ray diffraction pattern, suggesting that the DSC peak observed at 159 °C is associated with the structural relaxation of point defect and short-range order movement of atoms, as proposed by Hentschel *et al.*[22] Additionally, the presence of characteristic peaks associated with Ni and Ni_3P phases in the diffractogram of the sample heat treated at 400 °C is a clear indication that the DSC peak observed at 325 °C is related to the crystallization of the coating. However, it is not possible to identify characteristic peaks related to Cr metal or Ni-Cr-P alloys in these diffractograms. Finally, the diffractogram of the Cu/$Ni_{66}Cr_{12}P_{22}$-coated sample heat treated at 600 °C shows that heat treatment at this temperature does not lead to precipitation of new crystalline phase, suggesting that the DSC peak observed at 477 °C probably is associated with the structural relaxation of the crystalline structure. All these results are in close agreement with those obtained for sputtered Cu/Ni-Cr-P-coated samples[15] and sputtered AISI 420 steel/Ni-Cr-P-coated samples.[19]

The XRD diffractograms of Cu/Cr-coated samples, heat treated from 100 °C to 600 °C, were identical to that obtained for as-electrodeposited Cu/Cr-coated sample. All XRD diffractograms presented a characteristic peak at 2θ = 65° related to Cr (110).

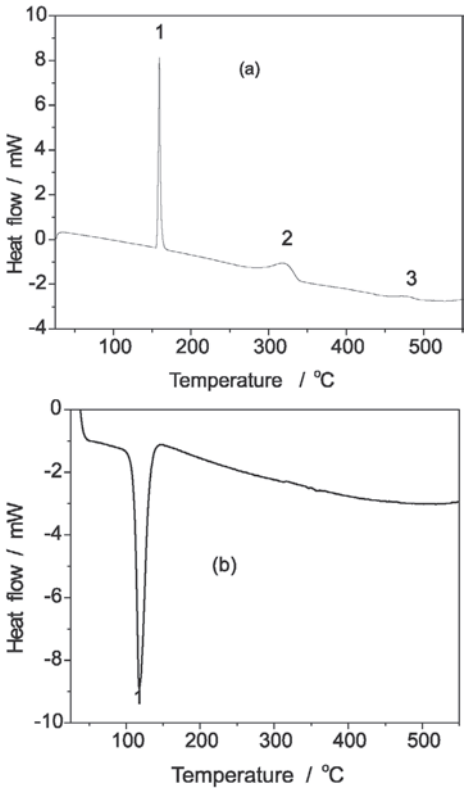

Figure 2. DSC plot of the $Ni_{66}Cr_{12}P_{22}$ (a) and Cr (b) coatings.

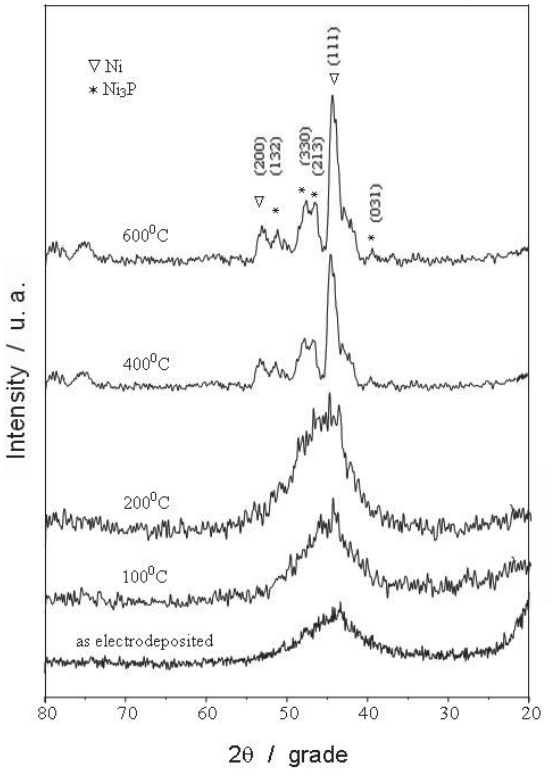

Figure 3. XRD diffraction patterns of the Cu/$Ni_{66}Cr_{12}P_{22}$-coated samples annealed at different temperature for 1 h.

Morphological investigation

The influence of the current density on the surface and cross section morphologies of the electrodeposited Ni-Cr-P and Cr coatings are shown in Figures 4 and 5, respectively. The SEM image of the Ni-Cr-P surface reveals the presence of spherical nodules on the surface, which are characteristic of electrodeposited Ni-P-based amorphous coatings.[10] Additionally, cracks are not observed on the surface coatings. The cross section micrograph (Figure 4f) shows a homogeneous and compact Ni-Cr-P coating without microcracks. These images suggest that the intense gas evolution during the electrodeposition does not produce internal stress in the coatings during the electrodeposition process, suggesting that these coatings can present better corrosion performance than other related electrodeposited Cr-iron-group-metal amorphous coatings reported in the literature, such as Fe-Cr-P-C,[9] Fe-Ni-Cr-P[10] and Fe-Cr-P-Co,[11] which present surface microcracks.

The surface morphology of Cr coating is characterized by dendrite microstructure (Figure 5a) while the cross-section micrograph reveals a homogeneous and compact coating without microcracks (Figure 5b). It is well known that a crack-free or a cracked morphology of electrodeposited Cr coating can be obtained by proper adjustment of the plating condition[24] and the morphologies shown in these micrographs are typical of electrodeposited Cr coatings obtained under this operational condition.

The influence of the annealing temperature in the surface and cross-section morphology of the selected $Ni_{66}Cr_{12}P_{22}$ coatings is presented in Figure 6. These SEM images show that the number of surfaces nodules is decreasing with the temperature and they are absent on the surface of the sample heat treated at 600 °C. Additionally, the absence of cracks was confirmed by the cross-section micrographs. On the other hand, the Cr coatings evolved to a cracked morphology from the surface until the substrate, as shown in Figure 7. The presence of cracks can be related to the internal stress of the coating developed during the heat treatment.

In order to understand the effect of the annealing temperature in the distribution of the elements in the coating, localized EDX analyses were carried out in the cross section of the $Ni_{66}Cr_{12}P_{22}$ coating at each 1 μm of thickness, from the substrate to the top, and the results are shown in Figure 8. Among all the obtained EDX spectra, just the one obtained on the top of the coating presented a peak related to the oxygen for both as-electrodeposited and as-annealed samples. The bigger peak associated with oxygen was observed in the EDX spectrum of the annealed Ni-Cr-P coatings, suggesting the formation of some surface Ni and Cr oxides thin films

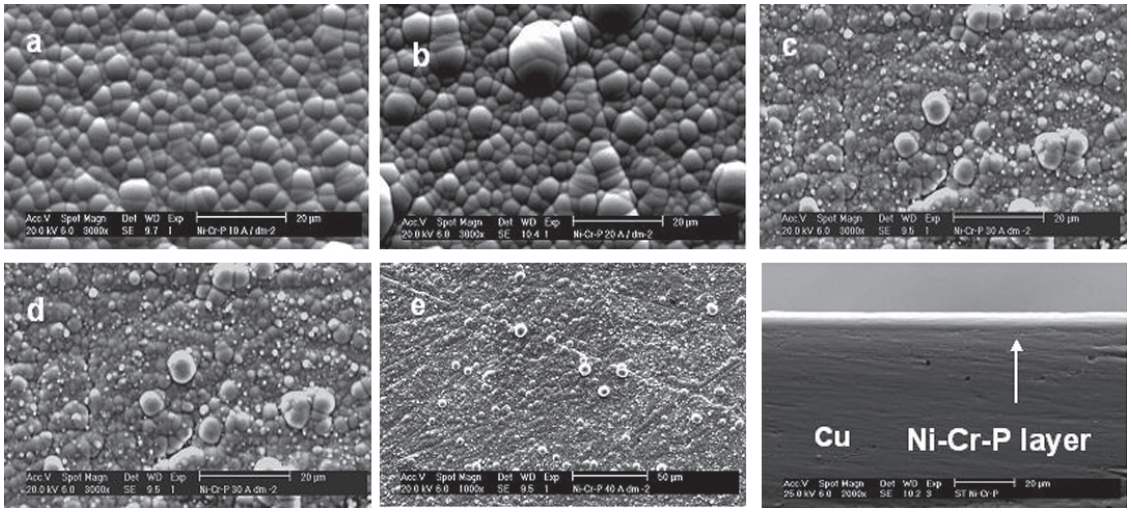

Figure 4. SEM micrographs showing the influence of the deposition current density on the surface morphology for Ni-Cr-P coatings obtained at 100 mA cm^{-2} (a), 200 mA cm^{-2} (b), 300 mA cm^{-2} (c), and 400 mA cm^{-2} (d,e). Cross-section micrograph of the sample obtained at 100 mA cm^{-2} is also shown (f).

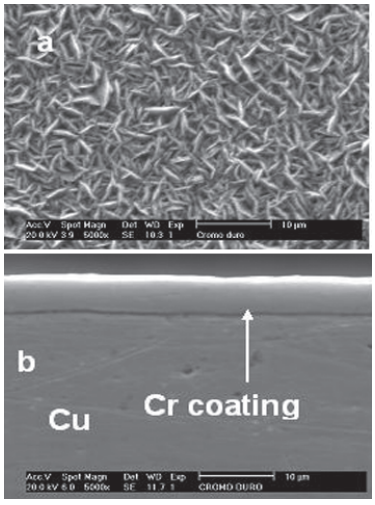

Figure 5. SEM micrographs showing the surface (a) and the cross-section (b) morphologies of the Cr coating.

under the annealing conditions used, which were not detected in the DRX analyses. The amount of the oxygen was not considered in the localized analysis of the cross-section of the Ni-Cr-P coatings.

In Figure 8, it is possible to observe that the as-electrodeposited samples presented uniform distribution of the elements in the coating. However, the heat treatment leads to a non-uniform distribution of the elements, since in the sample heat treated at 600 °C there is a significant increase of the Cr content from the substrate to the top while a decrease is observed for Ni and P contents from the substrate to the top. Thus, the EDX localized analyses suggest that a possible mechanism to explain the disappearance of the nodular structure with the annealing is the diffusion of Cr to the surface.

Microhardness measurements

Figure 9 shows the influence of the annealing temperature in the hardness of $Ni_{66}Cr_{12}P_{22}$ and Cr coatings. As it can be observed in this plot, as-electrodeposited $Ni_{66}Cr_{12}P_{22}$ coating presents lesser hardness value than as-electrodeposited Cr coating. However, the heat treatment leads to an increase in the hardness values of the Ni-Cr-P with the annealing temperature until 400 °C, remaining approximately constant for higher temperatures. On the other hand, the hardness values corresponding to the heat treated Cr coatings always decrease with the annealing temperature, indicating that the Cr coatings decrease in hardness in response to the presence of the cracks with the annealing. This hardness behavior observed for Ni-Cr-P coatings is in close agreement with those previously reported in the literature for sputtered Ni-Cr-P coating deposited on Cu substrate.[15,16] The increase of the hardness with the temperature is attributed to the crystallization hard compound Ni_3P, which was identified in the XRD of the Cu/$Ni_{66}Cr_{12}P_{22}$-coated sample heat treated at 400 °C and at 600 °C.

Electrochemical corrosion tests

The effect of Cr content in the corrosion behavior of the electrodeposited Ni-Cr-P coatings in 0.1 mol L^{-1} NaCl solution, at room temperature, it is shown in Figure 10, while the significant corrosion parameters derived from these curves are displayed in Figure 11. It can be observed in Figure 10 a reduction in the cathodic and in the anodic current densities with the increase of Cr content in the Ni-Cr-P coating. Additionally, Figure 11 shows that all

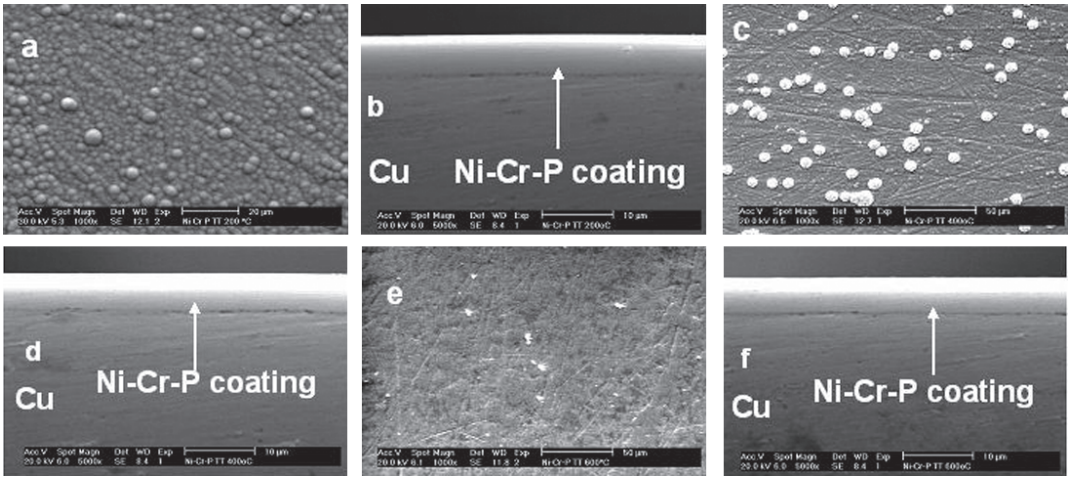

Figure 6. SEM micrographs of the surface and cross-section morphologies of $Ni_{66}Cr_{12}P_{22}$ coatings annealed at 200 °C (a,b), 400 °C (c,d) and 600 °C (e,f).

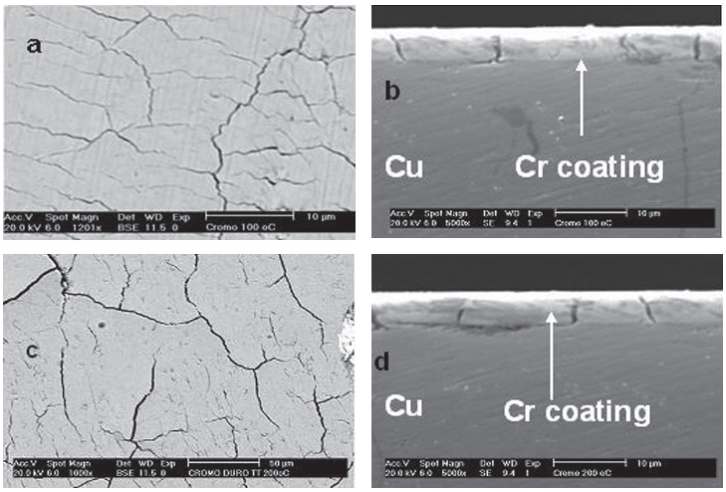

Figure 7. SEM micrographs of the surface and cross-section morphologies of Cr coatings annealed at 100 °C (a,b) and 200 °C (c,d).

electrodeposited Ni-Cr-P coatings exhibit a corrosion potential (E_{cor}) slightly positive in relation to that presented by the electrodeposited Cr coating, which shifts to less negative values with the increase of Cr content in the Ni-Cr-P coating. This is in close agreement with the investigation of Kang and co-workers[12,13] about the corrosion behavior of Fe-Ni-Cr-P-C alloys in 0.9 wt% NaCl solution. Additionally, the increase of the Cr content in the coating also leads to an increase of the polarization resistance (R_p) and the sample containing 12 at% Cr presenting similar Rp value to that presented by Cr coating.

As previously reported,[10] annealing is a process that is deleterious for the corrosion resistance of the electrodeposited amorphous alloys. Figure 12 shows typical polarization curves obtained for the selected $Ni_{66}Cr_{12}P_{22}$ and Cr coatings heat treated at 400 °C compared with those obtained for the corresponding as-electrodeposited Ni-Cr-P and Cr coatings. This figure shows that the annealing decreases the corrosion resistance of both coating, since as-annealed $Ni_{66}Cr_{12}P_{22}$ and as-annealed Cr coatings present higher cathodic and anodic current densities than the corresponding as-electrodeposited coatings. On the other hand, as-annealed $Ni_{66}Cr_{12}P_{22}$ coatings present lower anodic current densities than as-annealed Cr coating. Additionally, the values of the polarization resistance of the annealed $Ni_{66}Cr_{12}P_{22}$ coatings are always higher than the corresponding annealed Cr coatings, as shown in Figure 13. This figure also shows that the values of the polarization resistance of the annealed samples are smaller than as-electrodeposited samples.

Conclusions

Amorphous Ni-Cr-P alloys were successfully obtained by electrodeposition. The $Ni_{66}Cr_{12}P_{22}$ coating presented the best corrosion behavior of the various Ni-Cr-P coatings studied here. Cracks were observed in all annealed Cr coatings, while the morphology of

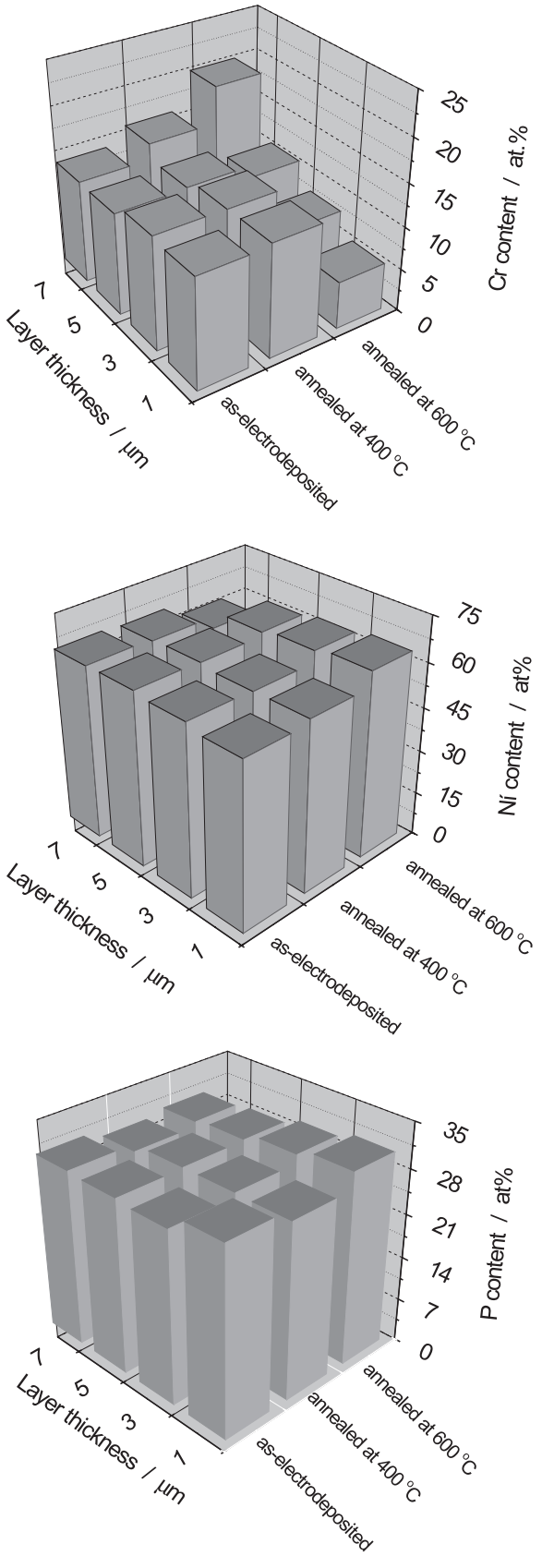

Figure 8. EDX analyses in the $Ni_{66}Cr_{12}P_{22}$ coating with the annealing temperature from the substrate to top.

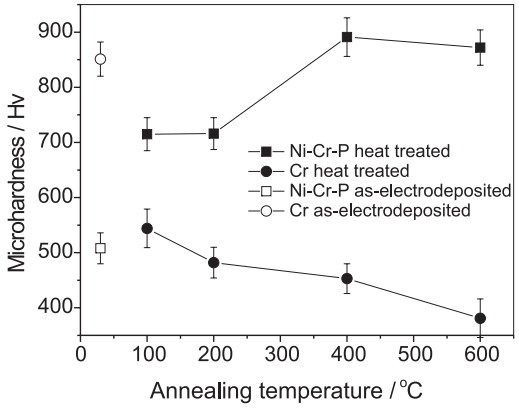

Figure 9. Evolution of the microhardness of the $Ni_{66}Cr_{12}P_{22}$ and Cr coatings as a function of annealing temperature.

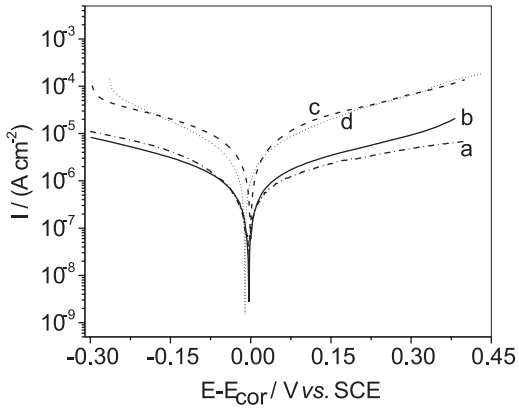

Figure 10. Potentiodynamic polarization curves obtained in 0.1 mol L^{-1} NaCl solution, at room temperature, and at 1 mV s^{-1} for as-electrodeposited Cr (a), $Ni_{66}Cr_{12}P_{22}$ (b), $Ni_{68}Cr_7P_{25}$ (c) and $Ni_{71}Cr_2P_{27}$ (d) coatings.

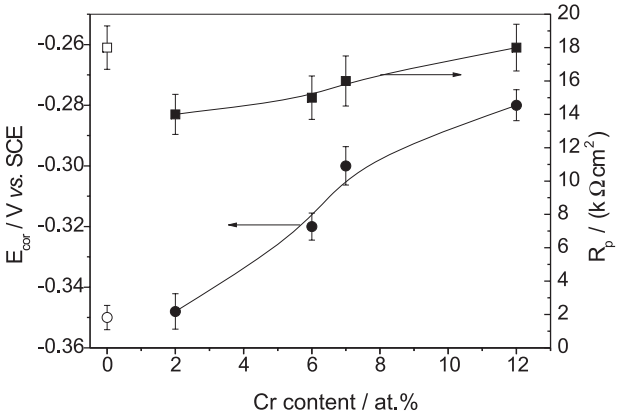

Figure 11. Dependence of the E_{cor} and R_p, derived from the polarization curves in 0.1 mol L^{-1}, with the Cr content in the electrodeposited Ni-Cr-P coatings (full symbols). The corresponding values for electrodeposited Cr coatings are presented (open symbols).

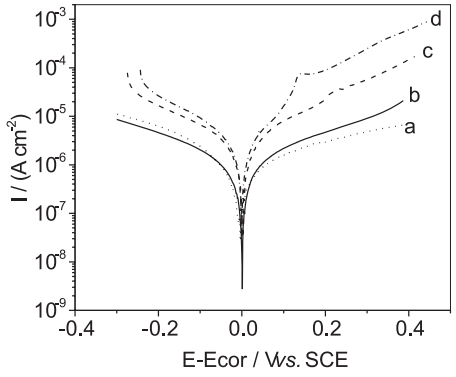

Figure 12. Potentiodynamic polarization curves obtained in 0.1 mol L-1 NaCl solution, at room temperature, and at 1 mV s-1 for the as-electrodeposited Cr (a) and $Ni_{66}Cr_{12}P_{22}$ (b) coatings and for the $Ni_{66}Cr_{12}P_{22}$ (c) and Cr (d) coatings annealed at 400 °C.

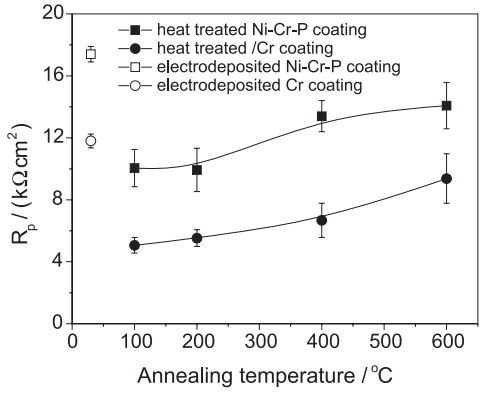

Figure 13. Dependence of the polarization resistance with the annealing temperature.

the annealed Ni-Cr-P coatings remained devoid of cracks. The nodular structure of the Ni-Cr-P coatings disappeared during annealing and it was associated with the diffusion of Cr to the surface. Crystallization of the Ni-Cr-P coating occurred at 325 °C with the formation of Ni and Ni_3P phases. The annealing at 400 °C and 600 °C caused precipitation of Ni_3P and Ni phases and the increase of the hardness of the Ni-Cr-P coatings. The hardness of the Cr coatings decreased with the rising of the annealing temperature. The presence of cracks impairs the mechanical and corrosion resistance properties of annealed Cr coatings. $Ni_{66}Cr_{12}P_{22}$ coatings can potentially replace Cr coatings in industrial applications, particularly at operational temperatures above room temperature.

Acknowledgments

The authors thank to CNPq, CNPq-CTPETRO (Proc. 460033/01-8), CAPES, FUNCAP and FINEP (Proc. 22.01.0762.00), Brazil, for financial assistance. Gecílio P. da Silva thanks to FUNCAP for the DSc scholarship.

References

1. Hoshino, S.; Laitener, H. A. G.; Hoflund, B.; *J. Electrochem. Soc.* **1986**, *133*, 681.
2. Brooman, E. W.; *Metal Finishing* **2004**, *102*, 42 and references cited therein.
3. Brooman, E. W.; *Metal Finishing* **2004**, *102*, 75 and references cited therein.
4. Safranek, W. H.; *The Properties of Electrodeposited Metals and Alloys*, American Elsevier Publishing Co., Inc.: New York, 1974.
5. Waseda, Y.; Aust, K. T.; *J. Matter. Sci.* **1981**, *16*, 2337.
6. Luborsky, F. E.; *Amorphous Metallic Alloys*, Butterworths: London, 1983.
7. Archer, M. D.; Corke, C. C.; Hargi, B. H.; *Electrochim. Acta* **1987**, *32*, 13.
8. Searson, P. C.; Nagarkar, P. V.; Latanision, R. M. In *Modern Aspects of Electrochemistry*; White, R. E.; Bockris, J. O'M.; Conway, B. E., eds.; Plenum Press: New York, 1990, vol. 21, p. 121.
9. Królikowski, A.; Butkiewicz, P.; *Electrochim. Acta* **1993**, *38*, 1979.
10. Parente, M. M. V.; Mattos, O. R.; Diaz, S. L.; Lima-Neto, P. de; Fabri-Miranda, F. J.; *J. Appl. Electrochem.* **2001**, *31*, 677.
11. Tsai, R. Y.; Wu, S. T.; *J. Electrochem. Soc.* **1991**, *138*, 1006.
12. Kang, J. C.; Lalvani, S. B.; *J. Appl. Electrochem.* **1992**, *22*, 787.
13. Kang, J. C.; Lalvani, S. B.; Melendres, C. A.; *J. Appl. Electrochem.* **1995**, *25*, 376.
14. Souza, C. A. C.; May, J. E.; Machado, A. T.; Tachard, A. L. R; Bidoia, E. D.; *Surf. Coat. Technol.* **2005**, *190*, 75.
15. Chen, W. Y.; Tein, S. K.; Wu, F. B.; Duh, J. G.; *Surf. Coat. Technol.* **2004**, *182*, 85.
16. Chen, W. Y.; Tein, S. K.; Duh, J. G.; *Surf. Coat. Technol.* **2004**, *188*, 489.
17. Lowenheim, F. A.; *Electroplating*, McGraw-Hill Book Company: New York, 1978.
18. Saiddington, J. P.; Hoey, G. R.; *J. Electrochem. Soc.* **1970**, *117*,1012
19. Saiddington, J. P.; Hoey, G. R.; *J. Electrochem. Soc.* **1973**, *120*, 1475.
20. Feliciano, L. E. T.; Oliveira, A. J. A. de; Schreiner, W. H.; Pereira, E. C.; *J. Electroanal. Chem.* **2005**, *574*, 333.
21. Dolati, A. G.; Ghorbani, M.; Afshar, A.; *Surf. Coat. Technol.* **2003**, *166*, 105.
22. Hentschel, T.; Isheim, D.; Kirchheim, R.; Müller, F.; Kreyer, H.; *Acta Mater.* **2000**, *48*, 933.
23. Dubpernell, G. In *Modern Electroplating,* 3th ed.; Lowenheim, F.A., ed.; Wiley-Intersicence Publication, John Wiley & Sons: New York, 1974.

Received: December 16, 2005
Published on the web: October 5, 2006